ATMOSPHERIC SCIENCE

Rapidly expanding nuclear arsenals in Pakistan and India portend regional and global catastrophe

Owen B. Toon[1]*, Charles G. Bardeen[2], Alan Robock[3], Lili Xia[3], Hans Kristensen[4], Matthew McKinzie[5], R. J. Peterson[6], Cheryl S. Harrison[7,8], Nicole S. Lovenduski[9], Richard P. Turco[10]

Pakistan and India may have 400 to 500 nuclear weapons by 2025 with yields from tested 12- to 45-kt values to a few hundred kilotons. If India uses 100 strategic weapons to attack urban centers and Pakistan uses 150, fatalities could reach 50 to 125 million people, and nuclear-ignited fires could release 16 to 36 Tg of black carbon in smoke, depending on yield. The smoke will rise into the upper troposphere, be self-lofted into the stratosphere, and spread globally within weeks. Surface sunlight will decline by 20 to 35%, cooling the global surface by 2° to 5°C and reducing precipitation by 15 to 30%, with larger regional impacts. Recovery takes more than 10 years. Net primary productivity declines 15 to 30% on land and 5 to 15% in oceans threatening mass starvation and additional worldwide collateral fatalities.

INTRODUCTION

The nuclear arsenals of Britain, France, China, Israel, India, and Pakistan are thought (*1*–*3*) to lie in the range of ~100 to 300 warheads each (Fig. 1). Although the use of these weapons by any of these countries could produce a regional, and likely global, disaster, India and Pakistan are of special concern because of a long history of military clashes including serious recent ones, lack of progress in resolving territorial issues, densely populated urban areas, and ongoing rapid expansion of their respective nuclear arsenals. Here, we examine the possible repercussions of a nuclear war between India and Pakistan circa 2025 in which cities are one class of target, either by direct or collateral targeting. These repercussions have not been investigated previously. Because of the near-term regional effects of nuclear blast, thermal radiation, and prompt nuclear radiation, we find that perhaps for the first time in human history, the fatalities in a regional war could double the yearly natural global death rate. Moreover, the environmental stresses related to climate changes caused by smoke produced from burning cities could lead to widespread starvation and ecosystem disruption far outside of the war zone itself.

Nuclear arsenals of India and Pakistan

The United States and Russia account for around 93% of the world's estimated 13,900 nuclear weapons. Seven other nuclear-armed nations are not bound by treaties that require them to divulge information, such as the number of strategic launchers and the number of warheads deployed on missiles, allowing estimates of the numbers of nuclear warheads and yields in their arsenals, but between them, the seven nations may now hold a total of 1200 warheads. As shown in Fig. 1, India's and Pakistan's nuclear forces in 2019 each may contain 140 to 150 warheads, with a possible expansion to 200 to 250 warheads in each country by 2025 (*1*, *3*–*5*). Britain (~215), France (~300), China (~270), and Israel (~80) have a similar number of weapons but have been maintaining relatively constant arsenals (*2*). Estimates of the numbers of warheads possessed by India and Pakistan are based on the capacity of delivery systems that can be observed from remote sensing, rather than on the amount of enriched uranium and plutonium fuel that the countries may have produced.

Pakistan has nuclear-capable aircraft (F-16A/B and Mirage III/V) with ranges up to 2100 km, eight types of land-based ballistic missiles with possible ranges up to 2750 km, and two types of cruise missiles with ranges up to 350 km (*4*, *6*). All of India can be reached by the longest-range delivery systems. Since India has about 400 cities with more than 100,000 people (*7*), Pakistan could potentially attack slightly more than one-third of all moderate- and large-sized cities in India with its current arsenal and more than two-thirds by 2025. Kristensen (*8*) provides satellite images and locations for 10 facilities in Pakistan that may be locations of missile garrisons or nuclear-capable fighter-bombers. Pakistan is developing capabilities for sea-based nuclear weapons. According to Pakistani officials, Pakistan's

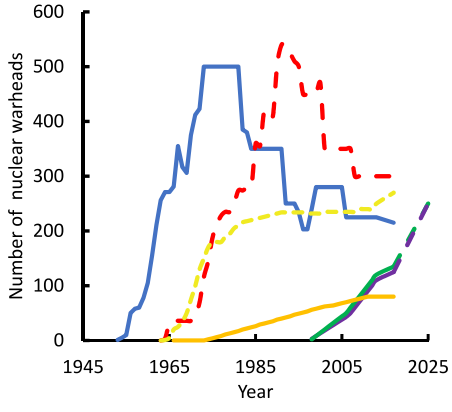

Fig. 1. The number of warheads thought to be in the arsenals of Britain (blue), France (red dashed), China (yellow dashed), India (purple), Pakistan (green), and Israel (orange) (*1*–*3*). North Korean weapons are not shown because it is uncertain whether they have an arsenal of useable weapons.

[1]Laboratory for Atmospheric and Space Physics, Department of Atmospheric and Oceanic Sciences, University of Colorado, Boulder, CO 80303, USA. [2]Atmospheric Chemistry Observations and Modeling Laboratory, National Center for Atmospheric Research, Boulder, CO 80307, USA. [3]Department of Environmental Sciences, Rutgers University, New Brunswick, NJ 08901, USA. [4]Federation of American Scientists, 1112 16th St., N.W. Suite 400, Washington, DC 20036, USA. [5]Natural Resources Defense Council, 40 West 20th St., 11th Floor, New York, NY 10011, USA. [6]Department of Physics, University of Colorado, Boulder, CO 80309-0390, USA. [7]School of Earth, Environmental, and Marine Sciences, University of Texas Rio Grande Valley, Port Isabel, TX 78597, USA. [8]Institute of Arctic and Alpine Research, University of Colorado, Boulder, CO 80309-0450, USA. [9]Department of Atmospheric and Oceanic Sciences, Institute of Arctic and Alpine Research, University of Colorado, Boulder, CO 80309-0450, USA. [10]Department of Atmospheric and Oceanic Sciences, University of California, Los Angeles, Los Angeles, CA 90095, USA.
*Corresponding author. Email: toon@lasp.colorado.edu

weapons are disassembled, and the parts are stored in several separate locations to reduce the possibility that terrorists might capture a usable weapon (*6*). Using satellite images, expert studies, and local news reports, Kristensen and Norris (*2*) identify nine locations in Pakistan where nuclear weapons may be stored.

On the basis of the sizes of weapons tested by Pakistan in 1998, it is estimated that the current weapons have yields of 5 to 12 kt (*6*, *8*). However, much higher yields are theoretically possible, which could greatly increase both casualties and global environmental effects. Pakistani scientists claim that all the weapons they tested in 1998 were uranium-based, boosted fission weapons that can have yields of hundreds of kilotons, without the need to develop more complex two-stage fission-fusion weapons. The 1998 tests did not demonstrate such high yields, and it is unknown whether Pakistan has been able to produce and deploy such high-yield warheads. Kristensen *et al.* (*4*) discuss the limited evidence of availability of tritium in Pakistan, which would be needed to allow boosted weapons to be produced. Advanced states are motivated to use boosted fission and two-stage weapons because they are smaller and lighter weight than fission weapons of the same yield, making them easier to deliver by missiles or aircraft. Boosted weapons also require less uranium or plutonium for a given yield.

Pakistan has produced tactical nuclear weapons for use on battlefields to counter the conventional weapons advantage of an invading Indian army. Their current arsenal probably includes 24 tactical weapons of unknown yield, but perhaps in the range of 5 to 12 kt (*6*). Tactical and strategic weapons (which are used to attack targets distant from a battlefield) can overlap in yield. The yields of advanced boosted fission weapons can be adjusted across a large range from sub-kilotons to more than 100 kt. Tactical weapons may be less secure than strategic ones and may lower the threshold for nuclear weapons use (*6*).

The 2018 arsenal of India is thought to contain 130 to 140 nuclear warheads, which may expand to 200 by 2025 (*5*). Kristensen and Norris (*2*) list five locations in India where nuclear weapons may be stored, but they estimate that there are others whose physical locations have not been identified.

India has nuclear-capable aircraft including Mirage 2000H and Jaguar IS/IB, with ranges up to 1850 km. It has four types of land-based ballistic missiles that have been deployed with ranges up to 3200 km and two others that are under development with ranges up to 5200 km. The range of these missiles allows India to reach all of Pakistan now, as well as all of China when its new missiles are deployed. India also has one deployed ship-based ballistic missile and two submarine-based missiles in development (*9*). Since Pakistan has about 60 cities with more than 100,000 people, India could potentially attack each moderate- or large-sized city in Pakistan with two nuclear warheads using its current arsenal and four warheads if its arsenal grows to 250 weapons by 2025.

On the basis of the sizes of weapons tested by India in 1998, the current weapons may have yields of 12 to 40 kt. However, higher yields are possible. India claims to have tested a two-stage weapon in 1998, but the recorded yield did not indicate a successful design. Kanwal (*10*), a retired Brigadier, examines the ideas of many Indian military leaders and suggests an Indian nuclear arsenal in 2011–2020 with 150 warheads, of which 134 have yields of 200 kt, whereas in 2021–2030, the arsenal might contain 200 warheads all of 200-kt yield. Although India does not need so many weapons to attack Pakistan, India is also concerned about China. China has about 360 cities with more than 100,000 inhabitants, so it is possible that India is sizing its nuclear forces in case of a nuclear conflict with China.

Scenario for war

Neither Pakistan nor India is likely to initiate a nuclear conflict without substantial provocation. India has declared a policy of no first use of nuclear weapons, except in response to an attack with biological or chemical weapons (*5*). Pakistan has declared that it would only use nuclear weapons if it could not stop an invasion by conventional means or if it were attacked by nuclear weapons. Unfortunately, the two countries have had four conventional wars (1947, 1965, 1971, and 1999) and many skirmishes with substantial loss of life since the partition of British India in 1947. Therefore, the possibility of conventional war becoming nuclear is of concern.

Lavoy and Smith (*11*) discuss three plausible scenarios for a nuclear war between India and Pakistan. India has conventional military superiority. India is also geographically much larger than Pakistan. One possible route to nuclear war involves a conventional conflict between India and Pakistan. If Pakistan perceived that India were about to successfully invade them, that would put pressure on Pakistan to launch its nuclear weapons before they were overrun by the superior conventional Indian forces. Another possibility for starting a nuclear conflict is that India or Pakistan could lose control of its command and control structures due to an attack on them by the other side or possibly an attack by terrorists from within India or Pakistan or from another country. In such a scenario, it is not clear who might be in control of the nuclear forces and what steps they might take. A third possibility for starting a nuclear conflict is that India or Pakistan might mistake an attack by conventional forces, or even military exercises, for an attack by nuclear forces.

To help evaluate the consequences of a nuclear conflict between India and Pakistan, table S1 provides a specific scenario for a war assumed to take place in 2025. Although this scenario has Pakistan first launching nuclear weapons, we do not mean to imply that they are more likely to do this than India. Because large numbers of weapons are assumed to be used by both sides, we would expect our results to be similar no matter how the war started. Moreover, we would expect the global outcomes projected here to apply equally well—with relevant recalibration for weapon sizes and targets and related smoke emissions—to any nuclear conflict between nuclear-armed states that involves a corresponding total yield detonated essentially in urban areas.

Many scenarios of an India-Pakistan conflict in 2025 are possible, ranging from no nuclear weapons deployed to as many as 500 nuclear weapons—many with yields above 100 kt—detonated. We chose the scenario outlined in table S1 as plausible following advice from a number of military and policy experts. In addition, the information presented in this paper and the Supplementary Materials can be used as a basis to compute the results for other scenarios. The main determinants of casualties and climate effects are the number of weapons used, the yield of the weapons, and the targets for the weapons, each of which is unknown in advance. The discussion in the following paragraphs exemplifies scenario factors that have been widely considered in the literature concerning conflicts between India and Pakistan, which might be varied in alternative scenarios including the role of the number of potential targets in choosing the sizes of arsenals; the characteristics, such as failure rates, of available weapons and delivery systems; the events that might lead to an escalating nuclear conflict; resolution of the Kashmir problem that might lessen

the likelihood of a dangerous confrontation; the importance of urban targets in contributing to fatalities and climate effects owing to high population densities and fuel loadings; the difficulty of preventing a conflict from going nuclear because of the destabilizing effects of tactical nuclear weapons on both sides; the importance of Indian concerns about China in making it difficult for Pakistan and India to reduce their nuclear stockpiles; and the possible role of the disproportionate sizes of the countries, militaries, and populations of India and Pakistan in motivating the initial use of nuclear weapons.

In the scenario outlined in table S1, we assumed that each country would have 250 nuclear weapons in 2025 (*5*, *9*). We also adopted a highly simplified scenario in which only urban targets are considered, and these are attacked using airbursts. Many military or strategic targets in rural areas are likely to be attacked as well, but these would involve smaller populations and lower fuel loading, which would not add significantly to the near-term fatalities or smoke emissions. Therefore, we do not specifically track them in our scenario. Likewise, some targets, such as buried military facilities, might attract ground bursts, which would produce significant radioactive fallout and many additional fatalities—effects that are not explicitly considered in this work.

India has one of the largest conventional militaries in the world, with about 1.4 million active duty personnel. India has not deployed tactical nuclear weapons. Indian nuclear strategy requires that a significant number of high-yield bombs be held back in case China joins a war on the side of Pakistan (*10*). Because Pakistan is a small country with only about 60 cities with more than 100,000 people, India would not need all of its 250 weapons to destroy Pakistan's cities.

We assume that India will keep 100 nuclear weapons in its arsenal to deter China from entering the war. Chinese involvement would greatly amplify the destruction discussed below. As China expands its presence in Pakistan as part of the China-Pakistan Economic Corridor, which is an element of China's broader "Belt and Road Initiative," the odds of a Pakistani-Indian war spreading to China would appear to be increasing.

Of India's 150 weapons that can be used against Pakistan, we assume that about 15% will fail. In this case, failure is primarily due to the weapons not being delivered or failing to explode. Most urban targets in Pakistan are so large that precise targeting is not needed to hit them. Therefore, our scenario suggests 125 weapons actually exploding. We further assume that there are 25 targets in Pakistan that are isolated military bases or industrial facilities located in regions with low populations and little combustible material. We do not include these in computing fatalities or environmental damage. Therefore, we assume that India has 100 strategic nuclear weapons to use on urban countervalue targets or military counterforce targets that are located within urban areas, such as military bases, industrial facilities, oil refineries, nuclear weapons facilities, and airports.

Pakistan also has one of the largest militaries in the world, with about half as many active duty personnel as India has. We assume that, in 2025, Pakistan will have 50 tactical weapons with yields of 5 kt to be used against an invading Indian army. We assume that 20% of these will fail or be overrun by the Indian Army. Many of these tactical weapons might be used in sparsely populated areas with little flammable material. Accordingly, we only consider the remaining 200 strategic weapons when computing fatalities or smoke created from fires. Of these 200 strategic weapons, we assume that 15% will fail to be delivered to the target but that the remaining 170 will be detonated over their targets. We further assume that 20 of these explosions will be over isolated military, nuclear, or industrial areas. The balance, 150 weapons, will thus be used against India's urban countervalue targets and military counterforce targets located within urban areas.

The yields of modern Indian and Pakistani weapons are unknown and not easily constrained. India detonated a ~40-kt yield weapon in 1998, which, they claimed, was a two-stage bomb. Kanwal (*10*) suggests that this design could produce 200-kt yields. Pakistan claimed that its weapons tested in 1998 used boosted fission. Possibly, these could also produce yields of 200 kt. Given the lack of reliable information about yield, we will explore the consequences of using strategic weapons with yields of 15, 50, and 100 kt.

Our scenario, as outlined in table S1, begins with a terrorist attack on the Indian government, similar to the one that occurred on 13 December 2001, but with massive fatalities among members of India's government. As happened in January 2002, we assume that India and Pakistan mobilize their troops within a few weeks of the terrorist attack. Indian troops would likely be dispersed along the border and in Kashmir. Skirmishes would break out, resulting in deaths on both sides. Similar skirmishes happened in 2002 and now occur with regularity, most recently with a conflict in the Kashmir region beginning with a terrorist event on 14 February 2019. In the 2002 confrontation, the United States, Russia, and other countries intervened, eventually convincing India and Pakistan to end the confrontation, which had continued into the summer of 2002 until Pakistan agreed to control terrorist groups within its borders.

A crisis simulation exercise in Sri Lanka during 2013 organized by the U.S. Naval Postgraduate School and involving retired senior military and civilian analysts from India and Pakistan found that "a limited war in South Asia will escalate rapidly into a full war with a high potential for nuclear exchange" (*12*). In our scenario, with the Indian government having been severely damaged, the Indian Army brings a number of tanks to the border and crosses into Pakistan and also crosses the Line of Control in Kashmir. On day 1 of the nuclear conflict, Pakistan uses 10 tactical atomic bombs with 5-kt yield inside its own borders with low air bursts against the Indian tanks (table S1).

The conflict continues on day 2 when Pakistan uses another 15 tactical weapons with 5-kt yield on the battlefield, whereas India detonates two air bursts against the Pakistani garrison in Bahawalpur and deploys 18 other weapons to attack Pakistani airfields and nuclear weapons depots, partially degrading Pakistani retaliatory capabilities. Nevertheless, on day 3, Pakistan responds with a barrage of nuclear ballistic and cruise missiles on garrisons, weapon depots, naval bases, and airfields in 30 locations in Indian cities (30 air bursts with 15- to 100-kt yield each) plus another 15 tactical bursts with 5-kt yield. India also uses 10 strategic weapons against Pakistani military bases on day 3. Because of panic, anger, miscommunication, and protocols, escalation cannot be stopped now. On days 4 to 7, cities in India are hit with 120 strategic weapons, and those in Pakistan are struck with 70 air bursts with 15- to 100-kt yield. In total, Pakistan's urban areas are hit with 100 nuclear weapons using airbursts, and India's urban areas are hit with 150 nuclear weapons using airbursts. In addition, Pakistan has used 40 tactical nuclear weapons successfully and 20 strategic weapons successfully on targets not in urban areas, whereas India has used 25 strategic weapons successfully on targets not in urban areas.

In previous simulations (*13*, *14*), all of the smoke produced during the nuclear exchange (as described below) was initially distributed

uniformly over a broad area of India and Pakistan in January 1. Here, the smoke is injected above individual targeted urban regions (at the grid scale of the climate model) on the day of the detonations. Hence, the smoke injection varies in location and time in accordance with the evolution of the specific war scenario (e.g., as illustrated in fig. S1 for the scenario with 50-kt weapons). Further, in the present climate simulations, the smoke injection is assumed to start on 15 May and extend over the duration of the exchange (e.g., 6 days for the case in fig. S1). We did not evaluate the sensitivity of the results to the time of year the war begins. In (*14*), it was found that a war initiated on 1 January or 15 May made little difference to the ultimate climatic effects. On the other hand, a war occurring in Northern Hemisphere summer might lead to enhanced impacts initially, as implied by earlier nuclear winter studies.

RESULTS

Near-term fatalities and casualties from nuclear explosions in India and Pakistan: Regional catastrophe

World War II experience

A considerable amount of information about the direct effects of nuclear explosions was gained from the nuclear attacks on Hiroshima and Nagasaki during World War II (WWII) and through the approximately 520 above-ground nuclear test explosions conducted before the 1963 Treaty banning nuclear weapons tests in the atmosphere, in outer space, and under water. Much of this information is summarized by Glasstone and Dolan (*15*) for generic topographical situations. Of course, the nuclear weapons tests took place in areas with little combustible material to prevent large-scale fires, so the tests provide little information about ignition of fires and fire behavior in urban areas. The area destroyed in the nuclear explosions over Japanese cities in WWII was greater in Hiroshima (yield, ~15 kt) than in Nagasaki (yield, ~20 kt), probably due to differences in topography (*15*). The bombed portion of Nagasaki is located in a valley, whereas Hiroshima is located in a flat terrain. Therefore, in reality, not all nuclear explosions follow the simple equations relating yields to destruction derived for flat terrain.

About 20 min after the Hiroshima nuclear explosion, a firestorm grew from the many small fires ignited directly or indirectly by the explosion. On the basis of the inflowing winds, the mass fire fully developed 2 to 3 hours after the explosion and died down around 6 hours after the explosion (*15*). The energy released in this mass fire may have been more than 1000 times greater than the energy released in the nuclear bomb blast (*16*). The area burned was about 11.4 km^2 according to Glasstone and Dolan (*15*) and 13 km^2 according to Ishikawa and Swain (*17*).

Regional nuclear war casualty estimates

Even one nuclear weapon explosion in a city can do a great deal of damage. For example, in the most densely populated urban area in Pakistan, a 15-kt airburst at the optimum height to maximize blast damage could kill about 700,000 people (fig. S2B) and injure another 300,000. With a 100-kt airburst over the same region, roughly 2 million fatalities and an additional 1.5 million nonfatal casualties could occur. Similar numbers would result for nuclear explosions over large Indian cities (fig. S2A).

Toon *et al.* (*16*) estimated that a war between India and Pakistan involving 50 nuclear weapons with 15-kt yield detonated as airbursts over the most densely populated cities of each nation would lead to about 22 million immediate fatalities and 44 million total casualties. Casualties include fatalities, severe injuries, and lesser injuries that can develop into more serious conditions, especially in the aftermath of a nuclear attack. At that time, it was assumed (*16*) that India had 85 (65 to 110) nuclear weapons and Pakistan had 52 (44 to 62), all with 15-kt yields. These casualty and fatality estimates were made using the LandScan2003 (*18*) population database together with the Gaussian probability distribution for fatalities and total casualties versus distance from ground zero shown in fig. S3 (*16*).

However, the urban populations of India and Pakistan are growing rapidly. The total urban populations of India and Pakistan are projected to increase by about 90% between 2000 and 2025, as shown in fig. S4 (*19*). The number of weapons possessed by the two countries is also thought to be increasing rapidly. By 2025, India and Pakistan could have three and five times, respectively, the number of weapons estimated by Toon *et al.* (*16*), and these would likely have higher yields than previously estimated (*16*).

We have recomputed the fatalities and casualties for the most recent Indian and Pakistani urban population counts using the approach discussed in Methods (see below) and in Toon *et al.* (*16*). Figure 2 illustrates the cumulative fatalities and cumulative total casualties as a function of the number of explosions and their yield derived using the LandScan2016 (*20*) population database. The corresponding fatalities calculated for individual targets are given in the Supplementary Materials (fig. S2). Cumulative fatalities (as well as overall casualties) are higher in India because it has a greater urban population. Fatalities are not linear with respect to the number, or yield, of the weapons used, because smaller cities (of which there are greater numbers) have lower populations, whereas higher-yield weapons on these targets would encounter low-density suburban or rural areas away from the city centers where lower-yield weapons concentrate most of their damage. Compared with India, Pakistani fatalities (fig. S2B) vary less with weapon yield above 15 kt, especially after the most densely populated 100 targets have been attacked, due to the relatively low populations of the remaining targets. India has many more moderate-sized cities than Pakistan, and fatalities continue to grow rapidly with yield above 15 kt, even for the 250th target (fig. S2A).

For 50 weapons of 15-kt yield exploding on both India and Pakistan, we find that the casualty estimates have risen relative to Toon *et al.* (*16*) from 22 to 27 million fatalities and from 44 to 45 million total casualties (Fig. 2) due to the expanded urban populations in LandScan2016 (*20*) compared to LandScan2003 (*18*). These increases in fatalities and casualties are much less than the ~50% increase in urban population between 2000 and 2015 (fig. S4), suggesting that the size of the area that is urban increases more than the population density within the urban region.

An even more marked increase in fatalities and casualties shown in Fig. 2 is due to increasing numbers of weapons and increasing yields. In Fig. 2, the targets are graphed in decreasing order of the population density within the target area [refer to Methods and (*16*)]. In the scenario outlined in table S1, Pakistan is assumed to use 150 strategic weapons on Indian urban targets and India is assumed to use 100 weapons on Pakistani urban targets. The calculations use the current population of India and Pakistan, not those for 2025, because it is not possible to forecast changing populations in individual target areas. Targets that are not in urban areas are not considered, but they would lead to additional fatalities and casualties. Table S2 lists the fatalities and casualties from the scenario given in table S1. About 50 million people would die if 15-kt weapons are used, almost 100 million if 50-kt weapons are used, and about 125 million if 100-kt weapons are used.

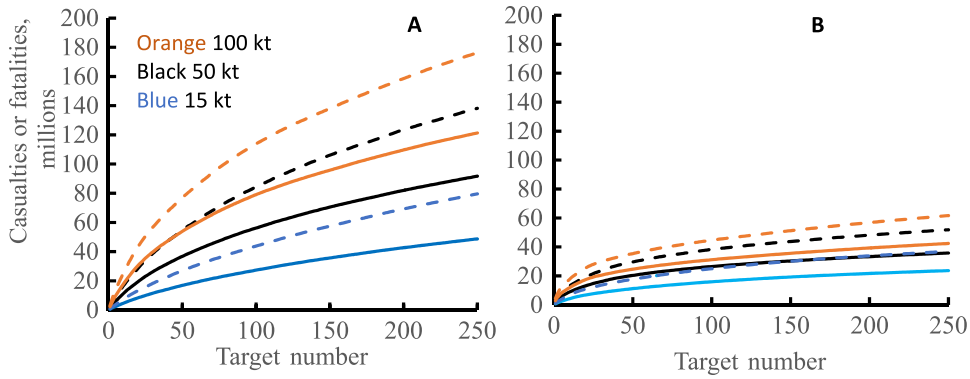

Fig. 2. The fatalities (solid lines) and total casualties (dashed lines) in millions, immediately following nuclear attacks, versus the number of targets. Results for India (**A**) and Pakistan (**B**). Colors corespond to the yield assumed.

The population density in the target area affects the casualties, as well as the estimated fuel load. Table S3 lists the population and population densities for the densest urban areas attacked and the least dense. The population density in the target area usually declines as the yield increases because more suburban areas are included in the larger areas that are damaged by higher-yield weapons. In some cases, especially for low-population regions in Pakistan, the population may decrease with yield because different urban areas are chosen as the last target for differing yields. The highest population densities in table S3 are in the range of 37,000 to 80,000 people/km^2. The population density in the area of the mass fire in Hamburg during WWII is estimated to have been about 20,000 people/km^2 (*21*). Similarly, the population density for the 150th weapon used on India is between 17,000 and 4900 people/km^2 and that for the 100th weapon used on Pakistan is between 8500 and 1600 people/km^2. For reference, the population density of 1980s San Jose, California, a suburban city, was estimated to be about 1300 people/km^2 (*16*).

During WWII, it is estimated that about 50 million people were killed, not considering those who died from disease and starvation over 6 years [e.g., (*22*)]. Because of the dense populations of cities in Pakistan and India, table S2 shows that even a war with 15-kt weapons could lead to fatalities approximately equal to those worldwide in WWII and a war with 100-kt weapons could directly kill about 2.5 times as many as died worldwide in WWII, and in this nuclear war, the fatalities could occur in a single week. The world's annual death rate from all causes is about 56 million people per year (*23*). Therefore, a war between India and Pakistan in our scenario with 15-kt weapons could kill the same number of people in a week as would die naturally worldwide in a year, effectively increasing the immediate global death rate by a factor of 50. A regional catastrophe would occur if India and Pakistan were to engage in a full-scale nuclear war with their expanding arsenals.

India would suffer two to three times more fatalities and casualties than Pakistan (table S2) because, in our scenario, Pakistan uses more weapons than India and because India has a much larger population and more densely populated cities. However, as a percentage of the urban population, Pakistan's losses would be about twice those of India. In general, as shown in Fig. 2, the fatalities and casualties increase rapidly even up to the 250th explosion due to the high population in India, whereas the rate of increase for Pakistan is much lower even for the 50th explosion.

The fatalities and casualties outlined in table S2, Fig. 2, and fig. S2 are computed, assuming airbursts used against urban targets, and that mass fires were started in each city, as occurred in Hiroshima. It is likely that some of the 45 strategic weapons assumed to be used against isolated military targets, and some of the 40 tactical weapons, will be exploded as ground bursts. The direct casualties and fatalities from ground bursts may be relatively small. However, ground bursts carry soil into the fireball, where very small radioactive particles can attach themselves to the dust particles. The relatively large dust particles are likely to fall out of the atmosphere within a few days, when the radioactive particles are still very dangerous. Large numbers of fatalities and casualties, potentially larger than the values given in table S2 and Fig. 2, can be caused by exposure to this radioactive material within a few days of the explosions.

Other considerations

Although the probability curves used here to determine fatalities and total casualties caused by airbursts have been crudely "calibrated" by the experience during WWII, the current estimates for a modern regional conflict involves a number of uncertainties that are difficult to reduce. Among the principal unknowns are the target points and the number and size of weapons used. There are many possible scenarios for a war, which can only be speculated upon in advance. Moreover, local environmental conditions—winds, humidity, precipitation, and so on—must be assumed from a wide range of possibilities. However, the core factual basis for the present estimates has been established through independent studies cited above. One can also question the use of probability curves based on data from Hiroshima in determining the ability of people in 21st-century cities to survive a nearby nuclear explosion. The probability curves adopted here correspond to physical processes triggered by nuclear detonations (principally thermal radiation and blast) that are likely to be lethal even in modern buildings and settings (fig. S3). We do not differentiate casualties between mass fires in high winds, where conflagrations occur and fire spread is likely (*24*, *25*), and mass fires in low winds, where firestorms develop and limited spreading is expected, as there is insufficient information available to make such a distinction quantitatively. Fire spread is likely to increase the ultimate casualty number, but it may also allow more people to flee from the fire.

Global climate perturbations due to nuclear conflict between India and Pakistan: Global catastrophe

Turco *et al.* (*26*, *27*) showed that smoke from fires started in cities by nuclear explosions could cool Earth's climate so much that agriculture would fail globally, leading to mass starvation. These early studies are supported by current climate model simulations (*28*, *29*).

Following a full-scale nuclear war involving the United States, Europe, Russia, and China using current arsenals, Toon *et al.* (*30*) estimated that 180 Tg (1 Tg = 1 Mt = 10^{12} g) of black carbon (BC) could be generated by a total of 4400 explosions of 100-kt weapons in urban areas, about half the arsenals of Russia, China, Britain, France, and the United States, assuming a yield that is lower than the average yield. Robock *et al.* (*28*), using a modern global climate model and assuming 150 Tg of smoke emitted in a superpower nuclear war [consistent with (*30*)], predicted a full-blown nuclear winter, with temperatures in mid-latitude grain-growing regions held below freezing for several years, destroying much of the world's agricultural productivity.

Robock *et al.* (*31*) and Toon *et al.* (*16*) showed that a conflict between India and Pakistan with 50 weapons of 15-kt yield used by each side that generated 5 Tg of BC would produce large climate changes as supported by additional studies with other models (*13*, *14*, *32*, *33*). Mills *et al.* (*13*, *14*) also found large ozone losses. These climate changes are large enough to significantly damage agriculture worldwide (*34*–*36*). Here, we compute the smoke-generated and climate changes for the scenario outlined in table S1 for possible Pakistani and Indian nuclear arsenals of 2025.

Smoke and BC (soot) emission estimates

As discussed by Toon *et al.* (*16*, *30*), we compute the amount and properties of smoke lofted to the upper troposphere in a sequence of steps, which are outlined below.

1. We first assume that the area subject to fire ignition for a 15-kt nuclear explosion is the same as that observed in Hiroshima (13 km^2). For different yields, we take the area subject to fire as proportional to the yield (*15*).

2. The fuel loading in the fire zone is determined using a recent population database (*20*) by allocating to each person in the area burned 11,000 kg of flammable material consisting of construction materials, furnishings, clothing, asphalt roofs, plastics, fuels, and other flammables in their homes, places of work, schools, stores, gas stations, and so on. This fuel allocation is based on studies of the quantities of combustible materials present in the developed world in the 1980s (*27*), as well as limited specific assessments of actual fuel availability in the relatively densely populated urban area of WWII Hamburg, Germany (various estimates yielding 12 to 47 g/cm^2), and more sparsely populated 1990 residential San Jose, California (1.34 g/cm^2) (*14*, *37*).

Reisner *et al.* (*38*) introduced a new technique to determine fuel loads in the United States using census data for urban fuels. Our estimated fuel load for their sparsely populated target location near Atlanta (0.87 g/cm^2) is within about 20% of their value. We have also used urban data from Washington, DC, to project a fuel load of 4 g/cm^2, which agrees within a few percentage with the mass per person estimated in (*27*). Larson and Small (*39*) suggested that, within the inner 2-km radius of urban cores in three classes of American cities circa 1980, fuel loadings were 23, 41, and 63 g/cm^2. Fuel loads in the major cities of Pakistan and India—summarized in table S3—are generally predicted to be in that same range. Unfortunately, less information is available to test these fuel values for Pakistan and India. Although Toon *et al.* (*16*) suggest that fuel burdens might be only half as large in the less developed world as in the developed world, this result is skewed by the inclusion of rural areas in the overall estimate. More directly, fuel loadings in Indian office buildings were found to be similar to those in British office buildings (*40*). In summary, considering the urban fuel loading models and data currently available, we conclude that there is a general, if somewhat tentative, consistency among the various studies mentioned above.

3. With regard to fire behavior, we assume that either (i) a firestorm would develop following a nuclear detonation in some number of cities, as happened at Hiroshima (and following the conventional bombing of Hamburg during WWII, for example), or (ii) a large-scale spreading conflagration would evolve in other urban areas, as happened with the conventional bombing of Tokyo and other cities during WWII. Further, in either case (i) or (ii), we assume that similar total quantities of fuel would eventually be consumed, and similar amounts of smoke would be lofted, after taking into account fire behavior (see the discussion below and also item 4). One characteristic that is not explicitly factored into our calculations is the difference in the period of time each type of fire would last, in general being longer for a conflagration as compared to a firestorm. This factor is not significant for the present global climate analysis.

Following Glasstone and Dolan (*15*), firestorms result when "many fires merge to form a single convective column ... rising from the burning area" and with "strong, fire-induced radial (inwardly directed) winds … virtually everything combustible within the firestorm area is eventually destroyed." On the basis of WWII experience with 69 mass fires in Japan and others in Germany, Glasstone and Dolan (*15*) conclude that firestorms can occur under the following conditions: a fuel loading of at least 4 g/cm^2, half the structures in an area aflame simultaneously, ambient winds less than 3.6 m/s, and a minimum burning area of about 1.3 km^2. For a 15-kt explosion, the minimum required fire ignition area is exceeded by roughly an order of magnitude. Table S3 also indicates that fuel loads needed to establish firestorms are generally exceeded, except in the case of large-yield weapons detonated over smaller Pakistani cities, where the requisite fuel load may be exceeded only within the city center. Moreover, it is clear that wind speeds may exceed the threshold for firestorm formation in some places at certain times. The WWII mass fires were generally much smaller than those that would be started by nuclear weapons considered here, so these firestorm conditions may not be applicable.

Mass fires, consisting of numerous fires burning simultaneously over a large area, may grow into massive conflagrations instead of firestorms when winds are high. Conflagrations have moving fire fronts and can continue to spread as long as there is sufficient fuel. High winds can drive and intensify such fires. Conflagrations, unlike firestorms, may be started at a single ignition point and are commonly associated with large forest fires burning along a widening frontal line. Conflagrations in forests generally consume readily ignitable fuels, such as the crowns of the trees and forest undergrowth, but not living tree trunks [for example, see (*41*, *42*)]. However, nuclear conflagrations in urban areas would likely be much more intense—owing to the many simultaneous starting points and heavy, highly flammable fuel loading. Moreover, given their propensity to spread outside of the initial ignition zone, conflagrations in urban settings could eventually consume as much fuel as a stationary firestorm, and perhaps more. Intense conflagrations are also observed to deposit smoke in the upper troposphere, and even the lower stratosphere, presumably by inducing strong pyroconvection at the fire front (*41*–*44*). Accordingly, both firestorms and conflagrations ignited by nuclear fireballs may ultimately have similar impacts on fuel consumption and, depending on fire intensity, smoke injection heights.

4. An important assumption in the present work is that all of the available fuel in the initial target-area fire zone is consumed when a firestorm develops. Although it is clear that this would be an upper limit, several factors mitigate toward this result. For example, accounts from WWII urban firestorms, such as those in Hiroshima and Hamburg, are consistent with nearly complete fuel consumption. Firefighting and suppression in nuclear attack zones would be effectively impossible, allowing fires to burn to completion. In addition, blast waves would release and disperse highly flammable fuels from storage tanks of all sizes, as well as piping and pipelines, and shatter and expose otherwise shielded fuels such as framing and building contents, leading to a more violent conflagration. Accordingly, the massive size and intensity of nuclear urban fires would most likely incinerate or pyrolyze a much larger fraction of available fuel than with smaller-scale localized combustion.

On the other hand, it is also likely that in blast-damaged regions of a city center, some otherwise available fuel would be covered by rubble and would not completely burn. In a nuclear airburst, reinforced concrete structures within the 140-kPa (20 psi) blast overpressure region can be destroyed. However, if the height of burst is optimized to produce such a blast pressure, the area of such destruction for a 15-kt airburst represents roughly 14% of the area within the 400,000 J m^{-2} (~10 cal cm^{-2}) fire ignition zone, and for a 100-kt blast, roughly 8%. Since, in most cases, the fuel density would be greater in the high overpressure zone, a larger fraction of the total fuel in the fire zone would be effectively buried—perhaps 20% or more, depending on the precise targets and weapons used. Owing to other sources of uncertainty in the fuel consumption estimation and the difficulty in determining a reasonable fuel sequestration factor due to rubble, we have ignored this effect in the current analysis until more information is available.

In the case of conflagrations, we allow that 50% of the fuel within the initial ignition zone would be burned, but that fire spread outside the area affected by thermal pulse would effectively double the fuel eventually consumed (*24*, *25*). These assumptions are not inconsistent with a significant impact on fuel consumption due to rubble formation in the blast zone.

5. We use an average BC (or soot) emission factor for burned fuel based on studies summarized by Turco *et al.* (*26*), yielding 0.02 g BC/g fuel burned. The less-absorbing organic carbon fraction of smoke that is typically mixed with the BC is ignored here. Other independent estimates of the total mass of emitted smoke may or may not include the mass of organic carbon in addition to BC. Accordingly, some care must be taken in comparing smoke estimates from different sources, as well as those quoted in assessments of impacts. The measured BC fraction of smoke can range widely from close to 90% to less than a few percentage, depending on the material burned and the flaming conditions that apply. For example, flaming combustion in forest fires may have a modest BC component, whereas the smoldering smoke has very little BC. On the other hand, burning fossil fuels have very high BC content. Our adopted average BC emission factor above has been derived by considering the range of fuel types and combustion conditions expected under nuclear attack scenarios (*16*, *26*, *27*, *45*).

6. Considering several studies summarized in (*16*, *27*), we assume that smoke generated by all nuclear bomb fires is initially injected into the 300- to 150-hPa pressure region of the upper troposphere (~9 to ~13.5 km). For latitudes from the equator to 35°N in the area of India and Pakistan, the cold point tropopause is in the 16- to 19-km altitude range (*46*). Therefore, we do not inject any smoke directly into the stratosphere. However, any smoke that might stabilize in the lower troposphere may be lofted too high.

7. On the basis of limited observations of pyrocumulus clouds (*16*), we assume that 20% of the BC is removed by rainfall during injection into the upper troposphere. Further smoke is rained out by the climate model before the smoke is lofted into the stratosphere by solar heating of the smoke. The fraction of the injected mass that is present in the model over 15 years is shown in fig. S5. In the first few days after the injection, 10 to 15% of the smoke is removed in the climate model before reaching the stratosphere. Therefore, in total, 30 to 35% of the smoke is removed by rainfall before it enters the stratosphere.

Uncertainty in smoke parameters

It is clear that imprecise knowledge regarding fire ignition and growth, and smoke composition, emission, and lofting, which are closely related to fuel loading and consumption, introduces significant uncertainty into all nuclear war climatic scenarios. Although all of these uncertain factors have been discussed extensively in the literature [e.g., (*16*, *26*, *27*, *47*)], some of the key parameters have not yet been sufficiently constrained to provide final assurance in climate predictions. Moreover, the parameterization of nuclear-initiated fires used in this work is, by necessity, highly simplified and not specific to any particular potential target. Nevertheless, there has been sufficient vetting of the physics and chemistry of potential nuclear warfare—including actual experience with nuclear attacks on cities in addition to large-scale testing, studies of basic processes under laboratory and field conditions, and theoretical modeling and analysis at all relevant spatial and temporal scales—that we consider the results presented here to be the most realistic currently possible.

There have been contrary assessments of the possible impacts of nuclear attacks on the global climate and environment. For example, most recently, a high-resolution modeling study (*38*) purported to demonstrate that a nuclear fire initiated by a 15-kt explosion in India or Pakistan would not loft enough smoke into the upper troposphere to contribute to widespread effects. However, that conclusion was based on a single simulation of such a detonation over a sparsely populated area about 8 km from the city center of Atlanta, Georgia. Significantly, the adopted fuel loading in the affected area (1.07 g/cm^2 in the ignition zone) was about one order of magnitude smaller than that in the most sparsely populated urban area considered in the present study, i.e., the 100th city attacked in Pakistan (refer to table S3). Accordingly, the preliminary findings in (*38*) are not representative of the fires that need to be considered in assessing the potential impacts of a conceivable nuclear conflict having regional or global extent.

Smoke emission scenarios

Because our global climate model has limited spatial and temporal resolutions compared to the scales of individual nuclear blast zones and fires, the smoke emissions determined for various attack scenarios have been inserted into the climate model, consistent with model resolution and the smoke parameterization described earlier.

Figure 3 shows the cumulative mass of BC that is inserted into the 300- to 150-hPa region (after rainout), with targets number-ordered by population. The BC emitted by individual targets is illustrated in fig. S2, which shows that, depending on yield, 10 to 25 targets in Pakistan and 15 to 125 cities in India could each produce more than 0.1 Tg of BC. Nuclear explosions in Pakistan generate far less BC than those in India for the same yield owing to the lower populations in Pakistan and the less dense urban areas after approximately

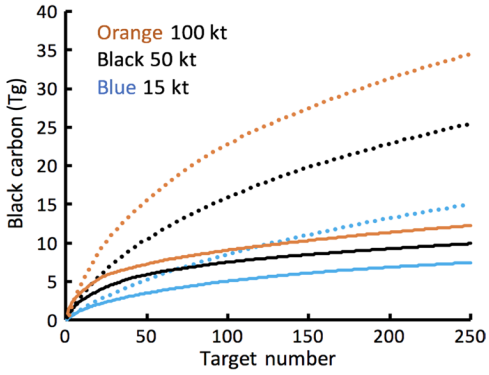

Fig. 3. Mass of black carbon (BC) injected into the atmosphere after prompt rainout (300- to 150-hPa region) for a given number of targets ordered by the population. Indian targets are given as dotted lines, whereas Pakistan targets are given as solid lines. Color coding designates yield.

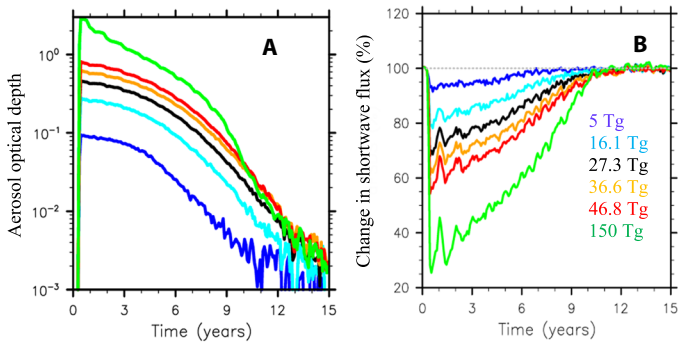

Fig. 4. Changes in amount of atmospheric aerosol and of solar energy at Earth's surface after nuclear exchange. Visible wavelength aerosol optical depth versus time (**A**) and the change in shortwave surface energy relative to normal as a function of time (**B**) for varying amounts of BC emitted in the nuclear exchange. Color coding designates the BC injection.

the 10 most populated cities are considered. The total BC emitted from a war in which 50 weapons with a 15-kt yield are used to attack each country is about 8.7 Tg. Toon *et al.* (*16*) estimated that 6.6 Tg would be generated using the LandScan2003 database. The 30% increase in predicted BC emissions between 2003 and 2016 is due to the growing urban populations over this period, as shown in fig. S4 (by ~50% between 2000 and 2016).

For the scenario in table S1 with 100 nuclear weapons used by India on Pakistan and 150 nuclear weapons used by Pakistan on India, there are (Fig. 3) 16.1 Tg of BC injected into the upper troposphere (11 from India and 5.1 from Pakistan) for yields of 15 kt, 27.3 Tg (19.8 from India and 7.5 from Pakistan) for 50-kt weapons, and 36.6 Tg (27.5 from India and 9.1 from Pakistan) for 100-kt weapons. These injection amounts are after considering the 20% removal of smoke by precipitation in the rising pyrocumulus.

These BC injections are of considerable concern for the climate. The greatest known natural injection of BC into the stratosphere of $\sim 6 \times 10^{-3}$ Tg occurred during August 2017 from forest fires in British Columbia (*42*, *43*). These fires led to radiatively forced rise of the smoke from 12 to above 23 km in about 2 months, radiatively driven hemispheric distribution of the smoke in the stratosphere, as well as temperature changes in the smoky layer due to heating by smoke, and ozone changes in the smoke due to vertical transport of low ozone air from the troposphere. The amount of BC in our 15-kt scenario is almost 3000 times more than in this forest fire injection.

In forest fires, only a small fraction of the fuel is consumed. The values for fuel burned in the British Columbia forest fire (*42*) are 10 to 25% of the fuel load expected in boreal forests. In addition, the accessible fuel loading is substantially lower in forests than in urban areas. In total, the fuel burned in the urban areas in our 15-kt scenario is about 60 times greater than estimated for typical forest fires. Our BC emission fractions are also about 50 times greater than in the forest fire case because the materials burned in urban mass fires produce more BC than does burning organic forest material in line fires.

Climate simulations

We have conducted a series of simulations using a configuration of the National Science Foundation/Department of Energy (DOE) Community Earth System Model (CESM) that is similar to that used in (*48*) to simulate the climate and atmospheric chemistry after the asteroid impact that killed the nonavian dinosaurs and many other species 66 million years ago by igniting most of Earth's land biomass and injecting about 15,000 Tg of BC into the upper atmosphere. A brief outline of this model is given in Methods.

Figure 4 shows the visible wavelength aerosol optical depth and the changes in solar energy at Earth's surface. There are results for six BC injections including the three scenarios defined in table S1 using possible yields of 15-, 50-, or 100-kt weapons, resulting in BC injections of 16.1, 27.3, and 36.6 Tg, respectively. The 5-Tg case is based on estimates made in 2008 for Indian and Pakistan arsenals at that time (*13*, *14*, *16*, *31*–*36*). The 46.8-Tg case would result from 250 weapons of 100-kt yield used against urban areas in India and Pakistan, which is likely an upper limit for a conflict between India and Pakistan, unless they have weapons with yields that are higher than 100 kt. By way of contrast with earlier nuclear winter scenarios, the green curves in Fig. 4 correspond to an injection of 150 Tg of BC over Russia and the United States, based on a scenario for a major nuclear war between these two superpowers (*28*–*30*).

The primary mechanism leading to climate changes after a nuclear conflict is absorption of solar radiation by smoke from burning cities. The direct solar beam is diminished in proportion to the inverse of the exponential of the aerosol optical depth. The initial global average aerosol optical depths range from less than 0.1 to greater than 2 for the cases considered in Fig. 4A. After 9 years, the 150-Tg optical depth is about equal to the initial optical depth of the 5-Tg case. The optical depth in the 150-Tg case is lower than some of the other cases after 10 years because the larger BC emission has led to the formation of larger particles via coagulation, and these have been more rapidly removed by sedimentation. The downward solar energy (Fig. 4B) reaching the surface declines in proportion to the increase of optical depth. The solar energy reaching the surface before the war is about 160 W m^{-2}. The fractional energy losses in Fig. 4B range from ~20 to 40% (~32 to ~64 W m^{-2}) for our conflict scenario (table S1) over the range of possible yields of 15-, 50-, or 100-kt weapons. For reference, the maximum average solar radiative loss following the Mt. Pinatubo volcanic eruption in 1991 was about 4 W m^{-2} (*49*), whereas the radiative reductions proposed for climate geoengineering schemes to offset global warming due to greenhouse gas emissions are of a similar magnitude. In addition, by comparison, a full-scale nuclear war between Russia and the United States might produce a peak solar radiation loss at the surface of ~75% (120 W m^{-2}) (*28*).

With a loss of solar radiation at the surface, the surface cools and evaporation, convection, and precipitation are reduced. Figure 5A

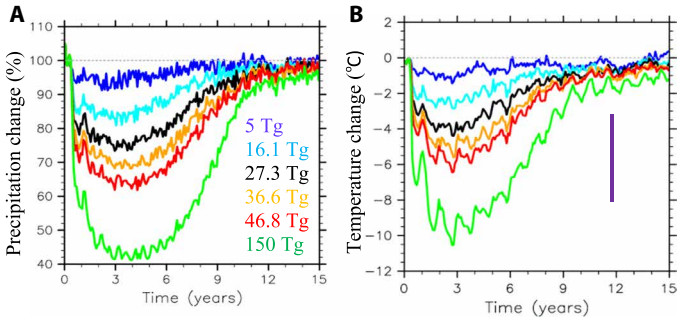

Fig. 5. Temporal variation in global precipitation and temperature following a nuclear conflict. (**A**) Global average precipitation and (**B**) global average temperature, expressed as a percentage of control run values. Color coding designates the amount of BC emitted. The vertical purple bar represents the range of temperatures during the height of the Last Glacial Maximum about 20,000 years ago.

indicates simulated global average precipitation losses from 15 to 30% for our scenario over the range of possible yields of 15-kt (16.1 Tg of BC), 50-kt (27.3 Tg), or 100-kt (36.6 Tg) weapons. A war between the United States and Russia could reduce precipitation by nearly 60%. Figure 5B shows that the global average surface temperature drops between 1.25° and 6.5°C over several years for our scenario. These perturbations reach their peak about 3 years after the conflict and are near the peak value for about 4 years. It takes more than a decade for temperatures and precipitation to return to normal. The Last Glacial Maximum, 20,000 years ago, had a global temperature decline of about 3° to 8°C relative to preindustrial temperatures, but these temperature decreases persisted for thousands of years (*50*).

Illustrations of postconflict temperature and precipitation anomalies over the major landmasses and oceans are presented in figs. S6 and S7. The average global land temperature (fig. S6B) declines by as much as ~4° to ~8°C for the present war scenario over the range of yields between 15 and 100 kt (BC emissions between 16 and 36 Tg). In contrast, annual average temperature decreases over land had been predicted to reach ~18°C for a full-scale nuclear winter. In the current scenario, globally averaged ocean surface temperatures (fig. S6A) decline by ~1 to almost 3°C for the range of yields assumed, whereas predicted anomalies reached ~6°C in the case of a superpower nuclear conflict. The ocean temperatures are expected to decrease in a layer extending roughly to the average thermocline depth [for example, as discussed in (*48*) for even larger smoke injections inferred at the geologic boundary marking the extinction of the dinosaurs]. Although cooling and precipitation reduction are global in scale, these changes vary regionally to a large extent. Postconflict temperature anomalies over land and ocean surfaces for the 50-kt (27.3 Tg) scenario are illustrated in fig. S6C, showing that cooling of the Northern Hemisphere continents is stronger than that of the Southern Hemisphere; temperature drops greater than 10°C occur across North America and Europe north of about 30° latitude, with cooling up to 5°C over all continents; ocean temperatures decrease in many regions by an average of 5°C, with greater reductions in the Northwest Atlantic. Similar spatial patterns of temperature anomalies were found for larger and smaller soot injections. Postconflict precipitation anomalies over land and oceans for the 50-kt (27.3 Tg) scenario are illustrated in fig. S7. Increased precipitation occurs in some areas, mainly because these regions are currently under the descending branches of the Hadley circulation. The descending air normally suppresses rainfall, but global cooling weakens the Hadley circulation, leading to more rainfall on average. Of greater significance to surviving populations are the large decreases in rainfall predicted over densely populated regions such as India and central China where precipitation almost ceases. The U.S. Northeast and Midwest lose more than 50% of their rainfall.

Although not illustrated here, and contrary to the response of temperatures at the surface, stratospheric air temperatures increase sharply because of sunlight absorption by injected BC (*31*–*33*). Such heating has previously been shown to cause large depletions of stratospheric ozone (*13*, *14*). It might be worth noting at this point that climate geoengineering proposals are based on reducing solar insolation by injecting stratospheric particles—such as sulfuric acid aerosol—that mainly scatter sunlight rather than absorbing it specifically to avoid the heating and ozone loss problem. However, sulfuric acid particles may still lead to ozone depletion through surface-catalyzed chemical reactions [e.g., (*13*, *14*)].

Impact on net primary productivity

One measure of the impact of these climate changes on life on Earth is the change in net primary productivity (NPP). NPP represents the net amount of inorganic carbon (mainly in the form of carbon dioxide) converted into organic plant matter through photosynthesis after accounting for plant respiration. NPP is typically expressed as grams of carbon per square meter per year (gC m^{-2} $year^{-1}$), where instantaneous rates of NPP may be scaled to equivalent annual values (*51*). Like the climate simulations, NPP is calculated here using the CESM, which includes both a land component [Community Land Model (CLM)] and ocean biogeochemistry module [Biogeochemical Elemental Cycling (BEC)]. These various models are more fully described in Methods. In CESM, NPP can be reduced on land through reductions in solar radiation, temperature, and precipitation. In the oceans, NPP can decrease in response to declines in solar radiation and temperature and may be further modified through associated changes in circulation and vertical mixing, which affect nutrient delivery and effective light availability.

Figure 6 (A and B) shows global ocean and land NPP variations, respectively, for a range of war scenarios. Globally integrated ocean NPP declines by a maximum of 10 to 20%, whereas terrestrial NPP can drop by 15 to 30% for several years for the range of yields between 15 and 100 kt (Fig. 6). NPP recovers after about 10 years. Imhoff *et al.* (*51*) estimated that the global annual land NPP is about 56.8 PgC/year (1 Pg = 10^{15} g). They further estimated that humans use 8.00 to 14.81 PgC/year or about 14 to 26% of NPP. Therefore, the projected loss of NPP is comparable to the total amount people use each year. In some regions, large fractions of local land NPP are appropriated by humans (*51*). For example, Western Europe uses 72%, south central Asia uses 80%, and East Asia uses 63% of NPP. Most of India, eastern China, parts of the Middle East, and areas of equatorial Africa consume more than 100% of local NPP. Hence, in these places, there is little or no margin for the loss of potential NPP following a regional nuclear conflict as described here.

For an India-Pakistan nuclear scenario using 50-kt weapons, terrestrial NPP reductions are much higher in the Northern Hemisphere than in the global average (Fig. 6, C and D), reaching 100% at latitudes north of about 60°N, averaged over the first 3 years after war. Major crop-growing regions of North America and Eurasia experience declines of NPP averaging 25 to 50% over this time. Very large reductions in NPP occur in India, China, Southeast Asia, and Indonesia, as well as in tropical South America and Africa. Ocean reductions in NPP are highest in the Arctic, where production is almost entirely

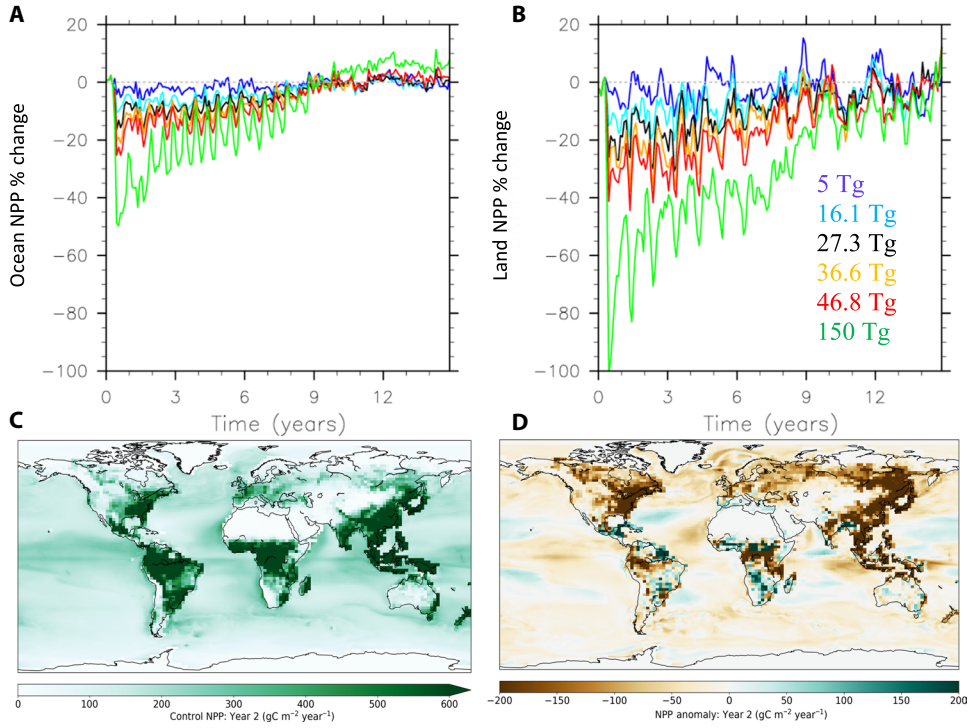

Fig. 6. Net primary productivity after nuclear war. Globally integrated monthly averaged NPP as a percentage of the baseline (control run) values as a function of time: over the oceans (**A**) and landmasses (**B**). Results are shown for each of the war scenarios described in the text. Color coding designates the corresponding BC injection amounts. As in Fig. 5, the full nuclear winter injection case (150 Tg, green line) is shown for contrast. (**C**) Global distribution of annual average NPP for the baseline control run. (**D**) Change from the baseline averaged over the second calendar year following a nuclear conflict, which starts in May of year 1 for the scenario with 50-kt weapons and a 27-Tg injection of BC.

extinguished. In addition, in many regions where major fisheries exist, production is significantly reduced, including the North Atlantic and North Pacific, where NPP decreases by 25 to 50%. Together, the reductions in temperature, primary productivity, and precipitation suggest major disruptions to human and natural systems worldwide.

DISCUSSION

India and Pakistan may be repeating the unfortunate example set by the United States and Russia during the "cold war" era: that is, building destructive nuclear forces far out of proportion to their role in deterrence. Should a war between India and Pakistan ever occur, as assumed here, these countries alone could suffer 50 to 125 million fatalities, a regional catastrophe. In addition, severe short-term climate perturbations, with temperatures declining to values not seen on Earth since the middle of the last Ice Age, would be triggered by smoke from burning cities, a global disaster threatening food production worldwide and mass starvation, as well as severe disruption to natural ecosystems. Compounding the devastation brought upon their own countries, decisions by Indian and Pakistani military leaders and politicians to use nuclear weapons could severely affect every other nation on Earth.

METHODS

To compute the number of fatalities and casualties from a nuclear detonation in a specific location, we numerically integrated the product of the spatially varying population density in that region and the probability of fatality or casualty as a function of distance from the detonation point, or "ground zero," using the probability distribution curves defined in fig. S3. Total fatalities and casualties for particular war scenarios were then determined by summing up the results from individual bursts. For a 15-kt weapon, we chose target sites by first calculating the total population within a 2-km radius around each grid cell in the LandScan2016 population database (*20*), where LandScan provides the 24-hour average population aggregated into cells that are 30 arc sec on a side—an area less than 1 km^2 at the latitudes of interest. Subsequently, we selected the most populated of these 2-km-radius regions as target points. However, we did not permit any of the 2-km zones to overlap, so that bursts are spatially well separated. Moreover, we did not consider the accumulated casualties from multiple bursts in overlapping damage zones. In practice, for the most densely populated regions, fatalities from the blast and thermal radiation of a 15-kt explosion did not occur beyond about 5 km from ground zero, and minor injuries did not occur beyond about 9 km (fig. S3). For yields greater than 15 kt, we took the affected area to scale linearly with yield and, thus, the population density target search radius scales as the nominal 2-km radius times the square root of the alternative yield divided by 15 kt [e.g., the 50-kt target population density was calculated over an area of $2 \times (50/15)^{1/2}$ ~3.7-km radius]. Further discussion of the target selection criteria and application to nuclear war scenarios can be found in our earlier work [e.g., (*16*)].

We used the CESM (*52*–*54*), a fully coupled climate model that includes atmosphere, ocean, land, and sea-ice components. We used the Whole Atmosphere Community Climate Model (WACCM), version 4, as the atmospheric component (*55*). WACCM is a "high-top" chemistry-climate model, with an upper boundary located near 140-km geometric altitude; it has a horizontal resolution of 1.9° × 2.5°

(latitude × longitude) and a variable vertical resolution averaging 1.25 km from the boundary layer to near 1 hPa, 2.5 km in the mesosphere, and 3.5 km in the lower thermosphere, above about 0.01 hPa. WACCM was used as the atmospheric model to be able to simulate the physical and chemical consequences of injection and lofting of BC to great heights in the atmosphere. To represent the evolution of a massive injection of smoke accurately, we coupled WACCM with the Community Aerosol and Radiation Model for Atmospheres (CARMA) (*56*). CARMA is a sectional aerosol parameterization that resolves the aerosol size distribution and allows the size distribution of the aerosols to evolve freely, which is necessary when simulating large aerosol injections, as in this study. CARMA aerosols are advected by WACCM, are subject to wet and dry deposition, affect the surface albedo when they are incorporated into snow, and are included in the WACCM radiative transfer calculation.

Soot was treated as a fractal aggregate for both microphysics and radiative transfer (*57*), and coagulation of soot particles was considered. The fractal particles have a monomer size of 30 nm, a fractal dimension varying between 1.5 and 3.0, and a packing coefficient of 1 (*57*). The shortwave optical properties of the fractal soot particles are dependent on monomer size, which is fixed at emission, but as observed (*58*) are largely independent of particle size, which does increase due to coagulation caused by the large soot emissions used in our simulations. The Rapid Radiative Transfer Model for General Circulation Models (RRTMG) (*59*), a radiation package within CESM, was used to include the radiative effects of the impact-generated aerosols. Optical properties for the soot aggregates were calculated using a mean field approximation (*60*) assuming a real refractive index of 1.95 and an imaginary refractive index of 0.79.

The burdens of soot aerosol considered here cause large temperature changes in the stratosphere and mesosphere, which required changes to WACCM to improve the numerical stability of the model as discussed by Bardeen *et al.* (*48*). We reported seven simulations for this study, a 20-year control simulation, and six experiments of 15-year duration each with varying amounts of soot injection.

Smoke is a complex mixture of BC (or soot) and a variety of organic compounds. In general, the organic material has a very low absorptivity at visible wavelengths. However, in addition to BC, some light-absorbing organic carbon in the form of "brown" carbon can be emitted by fires. The loss rates and mechanisms for brown carbon are poorly known, but lifetimes observed in the atmosphere are on the order of 1 day (*61*). Thus, although brown carbon would likely contribute to the short-term properties of smoke aerosol, it is not clear that it would be a significant long-term component of the smoke lofted into the stratosphere. Highly absorbing BC may compose only a few percentage of smoke from forest fires, even for smoke injected into the stratosphere (*43*, *62*). The remainder is composed of various forms of organic carbon. Much of the material consumed in urban fires is not composed of wood, and the wood that is consumed is dry and lacking much of the organic material in living wood. In addition, mass fires are much hotter than normal forest fires and may consume the organics in the fire. Organics are also subsequently oxidized by reaction with OH and ozone [for example, see (*43*)].

Recent observations of forest fire smoke in the stratosphere suggest that the organics are removed by chemical reactions with a lifetime of around 4 months (*43*). Because of the uncertainty in the emission rates and the added complexity in the chemistry of smoke organics, we did not include brown carbon or organic carbon in our simulations. Emissions of 45 Tg of organic carbon and 5 Tg of BC were included in simulations of regional nuclear war by Pausata *et al.* (*33*) who found that the added organics increase the surface cooling but that the larger particle size reduces the lifetime of the aerosols and, thus, the duration of the climate effects, from ~20 to ~10 years. Although it would be desirable to treat the smoke as an internal mixture of BC and organics, the emission factors for all of the smoke components and the oxidation pathways for the many organic components are poorly defined and beyond the current capabilities of our model. The optical depth of organic and/or water-coated soot particles can be about 1.5 times larger than for pure soot particles (*63*). Thus, our simulations may underestimate the total absorption of the soot particles; on the other hand, these particles would also be larger, with reduced lifetimes (*33*).

CESM version 1.3 is coupled with the ocean component known as the Parallel Ocean Program (POP) version 2 (*64*), with ocean biogeochemistry simulated by the BEC model (*65*), and the land component CLM version 4 (CLM4) with carbon-nitrogen cycle (CLM4CN) on (*66*). BEC includes three explicit phytoplankton functional groups (diatoms, diazotrophs, and picophytoplankton) and one implicit group (calcifiers) subject to multiple nutrient limitation (N, P, Si, and Fe) (*65*). Ocean net primary production is calculated as the sum of the carbon fixation by the three groups of phytoplankton over the top 150 m of the water column (*67*). CLM4CN specifies 15 plant functional types over vegetated land units and simulates vegetation changes with a fully prognostic treatment of the terrestrial carbon and nitrogen cycle, including interactions with biological mechanisms of plants and soil heterotrophs.

Our previous modeling of a nuclear conflict between India and Pakistan (*13*, *14*) differs in major alterations in the war scenarios and significantly in the mass of BC injected, as well as in the treatment of particle physics and optics. The scenario in table S1, for example, considers the projected arsenals in 2025, which are about five times larger than those of 2007 assumed in (*13*, *14*). We also treated a range of possible yields from 15 to 100 kt, whereas before, only 15-kt yields were used. Previously, smoke particles were assumed to be spherical with a fixed size of 50 nm; here, we allowed the size to vary, as particles coagulate to larger sizes and sediment with size-dependent fall velocities. We also allowed the particles to be fractal in structure with 30-nm monomers, as is observed in sooty smoke plumes. We, moreover, modified particle refractive indices to reflect currently accepted values for BC.

SUPPLEMENTARY MATERIALS

Supplementary material for this article is available at http://advances.sciencemag.org/cgi/content/full/5/10/eaay5478/DC1

Fig. S1. Urban targets in table S1 scenario for 50-kt weapons.
Fig. S2. Fatalities and BC emissions from individual targets.
Fig. S3. Probability of fatalities or casualties as a function of distance from ground zero.
Fig. S4. Estimated urban populations of India, Pakistan, and total for both nations.
Fig. S5. Fraction of the injected smoke remaining in the atmosphere as a function of time.
Fig. S6. Decline in ocean surface temperature and land surface temperature as a function of time.
Fig. S7. Global precipitation patterns and changes following a regional nuclear war.
Table S1. One scenario for a war between India and Pakistan.
Table S2. Fatalities and casualties and the percentage of the urban population killed or injured.
Table S3. Population densities within the area ignited and estimated fuel loads.

REFERENCES AND NOTES

1. H. M. Kristensen, M. Korda, *Status of World Nuclear Forces* (Federation of American Scientists, 2019); https://fas.org/issues/nuclear-weapons/status-world-nuclear-forces/.
2. H. M. Kristensen, R. S. Norris, Worldwide deployments of nuclear weapons, 2017. *Bull. At. Sci.* **73**, 289–297 (2017).

3. S. N. Kile, H. M. Kristensen, *Trends in World Nuclear Forces, 2017* (SIPRI Fact Sheet, 2017); sipri.org/sites/default/files/2017-06/fs_1707_wnf.pdf.
4. H. M. Kristensen, R. S. Norris, J. Diamond, Pakistani nuclear forces, 2018. *Bull. At. Sci.* **74**, 348–358 (2018).
5. H. M. Kristensen, M. Korda, Indian nuclear forces, 2018. *Bull. At. Sci.* **74**, 361–366 (2018).
6. H. M. Kristensen, R. S. Norris, Pakistani nuclear forces, 2016. *Bull. At. Sci.* **72**, 368–376 (2016).
7. O. B. Toon, A. Robock, M. Mills, L. Xia, Asia treads the nuclear path, unaware that self-assured destruction would result from nuclear war. *J. Asian Studies* **76**, 437–456 (2017).
8. H. M. Kristensen, Pakistan's evolving nuclear weapons infrastructure. *FAS Strategic Security Blog*, November 16 (2016); https://fas.org/blogs/security/2016/11/pakistan-nuclear-infrastructure.
9. H. M. Kristensen, R. S. Norris, Indian nuclear forces, 2017. *Bull. At. Sci.* **73**, 205–209 (2017).
10. G. Kanwal, India's nuclear force structure 2025. Carnegie Endowment for International Peace (2016); carnegieendowment.org/2016/06/30/india-s-nuclear-force-structure-2015-pub-63988.
11. P. R. Lavoy, S. A. Smith, The Risk of Inadvertent Nuclear Use Between India and Pakistan. Strategic Insight II. ADA525408 (2003); www.dtic.mil/dtic/tr/fulltext/u2/a525408.pdf.
12. H. F. Khan, R. W. French, South Asian Stability Workshop: A crisis simulation exercise (Naval Postgraduate School Center on Contemporary Conflict Project on Advanced Systems and Concepts for Countering WMD Report Number 2013–008, 2013).
13. M. J. Mills, O. B. Toon, R. P. Turco, D. E. Kinnison, R. R. Garcia, Massive global ozone loss predicted following regional nuclear conflict. *Proc. Natl. Acad. Sci. U.S.A.* **105**, 5307–5312 (2008).
14. M. J. Mills, O. B. Toon, J. Lee-Taylor, A. Robock, Multidecadal global cooling and unprecedented ozone loss following a regional nuclear conflict. *Earth's Future* **2**, 161–176 (2014).
15. S. Glasstone, P. J. Dolan, *The Effects of Nuclear Weapons, Third edition* (United States Department of Defense, and Energy Research and Development Administration, 1977).
16. O. B. Toon, R. P. Turco, A. Robock, C. Bardeen, L. Oman, G. L. Stenchikov, Atmospheric effects and societal consequences of regional scale nuclear conflicts and acts of individual nuclear terrorism. *Atmos. Chem. Phys.* **7**, 1973–2002 (2007).
17. E. Ishikawa, D. L. Swain *Hiroshima and Nagasaki the Physical, Medical, and Social Effects of the Atomic Bombings* (Basic Books, 1981).
18. LandScanTM Global Population Database (Oak Ridge, TN: Oak Ridge National Laboratory, 2003); https://landscan.ornl.gov/downloads/2003.
19. United Nations Department of Economic and Social Affairs, Population Division, *World Urbanization Prospects: The 2018 Revision, File 3: Urban Population at Mid-Year by region, subregion and country, 1950–2050 (thousands)* (United Nations Department of Economic and Social Affairs, Population Division, 2018); https://esa.un.org/unpd/wup/Download/.
20. LandScanTM Global Population Database (Oak Ridge, TN: Oak Ridge National Laboratory, 2016); https://landscan.ornl.gov/downloads/2016.
21. K. A. Lucas, J. M. Orient, A. Robinson, H. Maccabe, P. Morris, G. Looney, M. Klinghoffer, Efficacy of bomb shelters: With lessons from the Hamburg firestorm. *South. Med. J.* **83**, 812–820 (1990).
22. M. Clodfelter, *Warfare and Armed Conflicts a Statistical Reference, Vol II 1900–1991* (McFarland and Co., 1992).
23. United Nations, World Mortality 2017, Data Booklet (ST/ ESA/SER.A/412). (United Nations Department of Economic and Social Affairs, Population Division, 2017); www.un.org/en/development/desa/population/publications/pdf/mortality/World-Mortality-2017-Data-Booklet.pdf.
24. F. J. Sanborn, Fire protection lessons of the Japanese attacks, in *Fire and the Air War*, H. Bond Ed. (National Fire Protection, 1946).
25. U.S. Strategic Bombing Survey, The effects of atomic bombs on Hiroshima and Nagasaki, in *Fire and the Air War*, H. Bond Ed. (National Fire Protection, 1946).
26. R. P. Turco, O. B. Toon, T. P. Ackerman, J. B. Pollack, C. Sagan, Nuclear winter: Global consequences of multiple nuclear explosions. *Science* **222**, 1283–1292 (1983).
27. R. P. Turco, O. B. Toon, T. P. Ackerman, J. B. Pollack, C. Sagan, Climate and smoke: An appraisal of nuclear winter. *Science* **247**, 166–176 (1990).
28. A. Robock, L. Oman, G. L. Stenchikov, Nuclear winter revisited with a modern climate model and current nuclear arsenals: Still catastrophic consequences. *J. Geophys. Res.* **112**, D13107 (2007).
29. J. Coupe, C. Bardeen, A. Robock, O. B. Toon, Nuclear winter responses to nuclear war between the United States and Russia in the whole atmosphere community climate model version 4 and the Goddard Institute for Space Studies ModelE. *J. Geophys. Res.* **124**, 8522–8543 (2019).
30. O. B. Toon, A. Robock, R. P. Turco, Environmental consequences of nuclear war. *Phys. Today* **61**, 37–42 (2008).
31. A. Robock, L. Oman, G. L. Stenchikov, O. B. Toon, C. Bardeen, R. P. Turco, Climatic consequences of regional nuclear conflicts. *Atmos. Chem. Phys.* **7**, 1973–2002 (2007).
32. A. Stenke, C. R. Hoyle, B. Luo, E. Rozanov, J. Gröbner, L. Maag, S. Brönnimann, T. Peter, Climate and chemistry effects of a regional scale nuclear conflict. *Atmos. Chem. Phys.* **13**, 9713–9729 (2013).
33. F. S. R. Pausata, J. Lindvall, A. M. L. Eckman, G. Svensson, Climate effects of a hypothetical regional nuclear war: Sensitivity to emission duration and particle composition. *Earth's Future* **4**, 498–511 (2016).
34. L. Xia, A. Robock, Impacts of a nuclear war in South Asia on rice production in mainland China. *Clim. Change* **116**, 357–372 (2013).
35. L. Xia, A. Robock, M. J. Mills, A. Stenke, I. Helfand, Decadal reduction of Chinese agriculture after a regional nuclear war. *Earth's Future* **3**, 37–48 (2015).
36. M. Özdoğan, A. Robock, C. J. Kucharik, Impacts of a nuclear war in South Asia on soybean and maize production in the Midwest United States. *Clim. Change* **116**, 373–387 (2013).
37. D. S. Simonett, T. N. Barrett, S. Gopal, F. J. Holsmuller, H. Veregin, Estimates of the magnitude and spatial distribution of combustible materials in urban areas: A case study of the San Jose Area, California. *Fire and Materials* **12**, 95–108 (1998).
38. J. Reisner, G. D'Angelo, E. Koo, W. Even, M. Hecht, E. Hunke, D. Comeau, R. Bos, J. Cooley, Climate impact of a regional nuclear weapons exchange: An improved assessment based on detailed source calculations. *J. Geophys. Res.: Atmos.* **123**, 2752–2772 (2018).
39. D. A. Larson, R. D. Small, Analysis of the Large Scale Urban Fire Environment, Part II. Parametric Analysis and Model City Simulations, Pacific-Sierra Res. Corp, Contract EMW-C-0747, Work Unit 2564E (1982).
40. S. Kumar, C. V. S. K. Rao, Fire loads in office buildings. *J. Struct. Eng.* **123**, 365–368 (1997).
41. M. Fromm, O. Torres, D. Diner, D. Lindsey, B. Vant Hull, R. Servranckx, E. P. Shettle, Z. Li, Stratospheric impact of the Chisholm pyrocumulonimbus eruption: 1. Earth-viewing satellite perspective. *J. Geophys. Res.* **113**, D08202 (2008).
42. D. A. Peterson, J. R. Campbell, E. J. Hyer, M. D. Fromm, G. P. Kablick III, J. H. Cossuth, M. T. DeLand, Wildfire-driven thunderstorms cause a volcano-like stratospheric injection of smoke. *npj Clim. Atmos. Sci.* **1**, 30 (2018).
43. P. Yu, O. B. Toon, C. G. Bardeen, Y. Zhu, K. H. Rosenlof, R. W. Portmann, T. D. Thornberry, R.-S. Gao, S. M. Davis, E. T. Wolf, J. de Gouw, D. A. Peterson, M. D. Fromm, A. Robock, Black carbon lofts wildfire smoke high into the stratosphere to form a persistent plume. *Science* **365**, 587–590 (2019).
44. J. Ditas, N. Ma, Y. Zhang, D. Assmann, M. Neumaier, H. Riede, E. Karu, J. Williams, D. Scharffe, Q. Wang, J. Saturno, J. P. Schwartz, J. M. Katich, G. R. McMeeking, A. Zahn, M. Hermann, C. A. M. Brenninkmeijer, M. O. Andreae, U. Pöschl, H. Su, Y. Cheng, Strong impact of wildfires on the abundance and aging of black carbon in the lowermost stratosphere. *Proc. Natl. Acad. Sci. U.S.A.* **115**, E11595–E11603 (2018).
45. R. D. Small, Atmospheric smoke loading from a nuclear attack on the United States. *Ambio* **18**, 377–383 (1989).
46. S. V. Sunilkumar, A. Babu, K. Parameswaran, Mean structure of the tropical tropopause and its variability over the Indian longitude sector. *Climate Dynam.* **40**, 1125–1140 (2013).
47. A. B. Pittock, T. P. Ackerman, P. J Crutzen, M. C. MacCraken, C. S. Shapiro, R. P. Turco, *Environmental Consequences of Nuclear War SCOPE-28, Vol. 1, Physical and Atmospheric Effects* (Wiley, 1985, ed. 2, 1989).
48. C. G. Bardeen, R. R. Garcia, O. B. Toon, A. J. Conley, On transient climate change at the Cretaceous–Paleogene boundary due to atmospheric soot injections. *Proc. Natl. Acad. Sci. U.S.A.* **114**, E7415–E7424 (2017).
49. P. Minnis, E. F. Harrison, L. L. Stow, G. G. Gibson, F. M. Den, D. R. Doelling, W. L. Smith Jr., Radiative climate forcing by the Mount Pinatubo eruption. *Science* **259**, 1411–1415 (1993).
50. V. Masson-Delmotte, M. Schulz, A. Abe-Ouchi, J. Beer, A. Ganopolski, J. F. González Rouco, E. Jansen, K. Lambeck, J. Luterbacher, T. Naish, T. Osborn, B. Otto-Bliesner, T. Quinn, R. Ramesh, M. Rojas, X. Shao, A. Timmermann, Information from Paleoclimate Archives, in *Climate Change 2013: The Physical Science Basis. Contribution of Working Group I to the Fifth Assessment Report of the Intergovernmental Panel on Climate Change*, T. F. Stocker, D. Qin, G.-K. Plattner, M. Tignor, S. K. Allen, J. Boschung, A. Nauels, Y. Xia, V. Bex, P. M. Midgley, Eds. (Cambridge Univ. Press, 2013).
51. M. L. Imhoff, L. Bounoua, T. Ricketts, C. Loucks, R. Harriss, W. T. Lawrence, Global patterns in human consumption of net primary production. *Nature* **429**, 870–873 (2004).
52. K. Lindsay, G. B. Bonan, S. C. Doney, F. M. Hoffman, D. M. Lawrence, M. C. Long, N. M. Mahowal, J. K. Moore, J. T. Randerson, P. E. Thornton, Preindustrial-control and twentieth-century carbon cycle experiments with the Earth System Model CESM1(BGC). *J. Climate* **27**, 8981–9005 (2014).
53. K. M. Krumhardt, N. S. Lovenduski, M. C. Long, K. Lindsay, Avoidable impacts of ocean warming on marine primary production: Insights from the CESM ensembles. *Global Biogeochem. Cycles* **31**, 114–133 (2017).
54. J. W. Hurrell, M. M. Holland, P. R. Gent, S. Ghan, J. E. Kay, P. J. Kushner, J.-F. Lamarque, W. G. Large, D. Lawrence, K. Lindsay, W. H. Lipscomb, M. C. Long, N. Mahowald, D. D. Marsh, R. B. Neale, P. Rasch, S. Vavrus, M. Verstenstein, D. Bader, W. D. Collins, J. J. Hack, J. Kiehl, S. Marshall, The community earth system model: A framework for collaborative research. *Bull. Am. Meteorol. Soc.* **94**, 1339–1360 (2013).

55. D. R. Marsh, M. J. Mills, D. E. Kinnison, J.-F. Lamarque, N. Calvo, L. M. Polvani, Climate change from 1850 to 2005 simulated in CESM1(WACCM). *J. Climate* **26**, 7372–7391 (2013).
56. C. G. Bardeen, O. B. Toon, E. J. Jensen, D. R. Marsh, V. L. Harvey, Numerical simulations of the three-dimensional distribution of meteoric dust in the mesosphere and upper stratosphere. *J. Geophys. Res.* **113**, D17202 (2008).
57. E. T. Wolf, O. B. Toon, Fractal organic hazes provided an ultraviolet shield for early Earth. *Science* **328**, 1266–1268 (2010).
58. J. Nelson, Fractality of sooty smoke: Implications for the severity of nuclear winter. *Nature* **339**, 611–613 (1989).
59. M. J. Iacono, E. J. Mlawer, S. A. Clough, J.-J. Morcrette, Impact of an improved longwave radiation model, RRTM, on the energy budget and thermodynamic properties of the NCAR community climate model, CCM3. *J. Geophys. Res.* **105**, 14873–14890 (2000).
60. R. Botet, P. Rannou, M. Cabane, Mean-field approximation of Mie scattering by fractal aggregates of identical spheres. *Appl. Optics* **36**, 8791–8797 (1997).
61. H. Forrister, J. Liu, E. Scheuer, J. Dibb, L. Ziemba, K. L. Thornhill, B. Anderson, G. Diskin, A. E. Perring, J. P. Schwarz, P. Campos-Jost, D. A. Day, B. B. Palm, J. L. Jimenez, A. Nenes, R. J. Weber, Evolution of brown carbon in wildfire plumes. *Geophys. Res. Lett.* **42**, 4623–4630 (2015).
62. P. Yu, O. B. Toon, C. G. Bardeen, A. Bucholtz, K. H. Rosenlof, P. E. Saide, A. Da Silva, L. D. Ziemba, K. L. Thornhill, J.-L. Jimenez, P. Campuzano-Jost, J. P. Schwarz, A. E. Perring, K. D. Froyd, N. L. Wagner, M. J. Mills, J. S. Reid, Surface dimming by the 2013 Rim Fire simulated by a sectional aerosol model. *J. Geophys. Res. Atmos.* **121**, 7079–7087 (2016).
63. M. Z. Jacobson, A physically-based treatment of elemental carbon optics: Implications for global direct forcing of aerosols. *Geophys. Res. Lett.* **27**, 217–220 (2000).
64. R. D. Smith, P. Jones, F. Bryan, G. Danabasoglu, J. Dennis, J. Dukowicz, C. Eden, B. Fox-Kemper, P. Gent, M. Hecht, S. Jayne, M. Jochum, W. Large, K. Lindsay, M. Maltrud, N. Norton, S. Peacock, M. Vertenstein, S. Yeager, The Parallel Ocean Program (POP) reference manual (Tech. Rep. LAUR-10-01853) (Los Alamos National Laboratory, 2010); www.cesm.ucar.edu/models/cesm1.0/pop2/doc/sci/POPRefManual.pdf.
65. J. K. Moore, K. Lindsay, S. C. Doney, M. C. Long, K. Misumi, Marine ecosystem dynamics and biogeochemical cycling in the community earth system model [CESM1(BGC)]: Comparison of the 1990s with the 2090s under the RCP4.5 and RCP8.5 scenarios. *J. Climate* **26**, 9291–9312 (2013).
66. K. W. Oleson, D. M. Lawrence, G. B. Bonan, M. G. Flanner, E. Kluzek, P. J. Lawrence, S. Levis, S. C. Swenson, P. E. Thorton, A. Dai, M. Decker, R. Dickinson, J. Feddema, C. L. Heald, F. Hoffman, J.-F. Lamarque, N. Mahowald, G.-Y. Niu, T. Qian, J. Randerson, S. Running, K. Sakaguchi, A. Slater, R. Stöckli, A. Wang, Z.-L. Yang, X. Ze, X. Zeng, Technical description of version 4.0 of the Community Land Module (CLM), (*NCAR Technical Note* NCAR/TN-478+STR, 257pp., National Center for Atmospheric Research, Boulder, CO., 2010).
67. C. S. Harrison, M. C. Long, N. S. Lovenduski, J. K. Moore, Mesoscale effects on carbon export: A global perspective. *Global Biogeochem. Cycles* **32**, 680–703 (2018).

Acknowledgments: This work used the RMACC Summit supercomputer, which was supported by the NSF (awards ACI-1532235 and ACI-1532236), the University of Colorado Boulder, and Colorado State University. The Summit supercomputer is a joint effort of the University of Colorado Boulder and Colorado State University. Part of this product was made using the LandScan (2016) High-Resolution Global Population Data Set copyrighted by UT-Battelle LLC, operator of Oak Ridge National Laboratory under contract no. DE-AC05-00OR22725 with the U.S. DOE. The U.S. Government has certain rights in this dataset. Neither UT-Battelle LLC, nor the U.S. DOE, nor any of their employees makes any warranty, express or implied, or assumes any legal liability or responsibility for the accuracy, completeness, or usefulness of the dataset. **Funding:** This work was funded by the Open Philanthropy Project. **Author contributions:** O.B.T., C.G.B., A.R., and R.P.T. wrote the manuscript. R.J.P. provided the initial idea for the paper. O.B.T., C.G.B., A.R., H.K., and M.M. devised the scenario. C.G.B. and C.S.H. performed model simulations. L.X., C.S.H., and N.S.L. provided analysis and insights into NPP and ocean physics. All authors edited the manuscript. **Competing interests:** The authors declare that they have no competing interests. **Data and materials availability:** The source code for the WACCM/CARMA model used in this study is freely available at www2.cesm.ucar.edu/ upon registration. All data needed to evaluate the conclusions in the paper are present in the paper and/or the Supplementary Materials. The data that form or illustrate the key results or images for this paper are available at Toon_2019_India_Pakistan retrieved from osf.io/pydf8. Additional information related to this paper, such as the evolving version of the model, as well as the input data and files necessary to reproduce our specific experiments, may be requested from the authors.

Submitted 27 June 2019
Accepted 9 September 2019
Published 2 October 2019
10.1126/sciadv.aay5478

Citation: O. B. Toon, C. G. Bardeen, A. Robock, L. Xia, H. Kristensen, M. McKinzie, R. J. Peterson, C. S. Harrison, N. S. Lovenduski, R. P. Turco, Rapidly expanding nuclear arsenals in Pakistan and India portend regional and global catastrophe. *Sci. Adv.* **5**, eaay5478 (2019).